



This is a repository copy of *Recombination processes in MBE grown Al_{0.85}Ga_{0.15}As_{0.56}Sb_{0.44}*.

White Rose Research Online URL for this paper:
<https://eprints.whiterose.ac.uk/200668/>

Version: Published Version

Article:

Gandan, S. orcid.org/0000-0001-6126-0699, Pinel, L.L.G. orcid.org/0000-0001-8603-5631, Morales, J.S.D. orcid.org/0000-0003-0401-324X et al. (3 more authors) (2023) Recombination processes in MBE grown Al_{0.85}Ga_{0.15}As_{0.56}Sb_{0.44}. AIP Advances, 13 (4). 045010. ISSN 2158-3226

<https://doi.org/10.1063/5.0145051>

Reuse

This article is distributed under the terms of the Creative Commons Attribution (CC BY) licence. This licence allows you to distribute, remix, tweak, and build upon the work, even commercially, as long as you credit the authors for the original work. More information and the full terms of the licence here:
<https://creativecommons.org/licenses/>

Takedown

If you consider content in White Rose Research Online to be in breach of UK law, please notify us by emailing eprints@whiterose.ac.uk including the URL of the record and the reason for the withdrawal request.



eprints@whiterose.ac.uk
<https://eprints.whiterose.ac.uk/>

Recombination processes in MBE grown $\text{Al}_{0.85}\text{Ga}_{0.15}\text{As}_{0.56}\text{Sb}_{0.44}$

Cite as: AIP Advances **13**, 045010 (2023); <https://doi.org/10.1063/5.0145051>

Submitted: 03 February 2023 • Accepted: 20 March 2023 • Published Online: 06 April 2023

 Shumithira Gandan,  Lucas L. G. Pinel,  Juan S. D. Morales, et al.



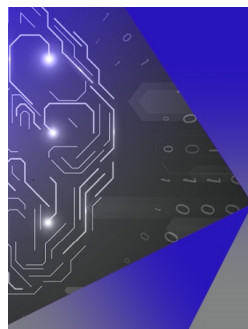
View Online



Export Citation



CrossMark



APL Machine Learning

Machine Learning for Applied Physics
Applied Physics for Machine Learning

**First Articles
Now Online!**

Recombination processes in MBE grown $\text{Al}_{0.85}\text{Ga}_{0.15}\text{As}_{0.56}\text{Sb}_{0.44}$

Cite as: AIP Advances 13, 045010 (2023); doi: 10.1063/5.0145051

Submitted: 3 February 2023 • Accepted: 20 March 2023 •

Published Online: 6 April 2023



View Online



Export Citation



CrossMark

Shumithira Gandan^{1,2a)}  Lucas L. G. Pinel,^{3,b)}  Juan S. D. Morales^{1,2}  Jo Shien Ng,³  Chee Hing Tan,³  and Tomasz Ochalski^{1,2} 

AFFILIATIONS

¹Centre of Advanced Photonics Process Analysis, Munster Technological University, Rossa Avenue, Bishopstown Cork, Ireland

²Tyndall National Institute, Dyke Parade, Cork City, Ireland

³Department of Electronic and Electrical Engineering, University of Sheffield, Sheffield, United Kingdom

a) Author to whom correspondence should be addressed: shumithirag@gmail.com

b) Current address: TMC Science and Technology, Da Vincilaan, Zaventem, Belgium.

ABSTRACT

Quaternary AlGaAsSb alloys have exhibited low excess noise characteristics as gain regions in avalanche photodiodes. In this work, optical spectroscopy techniques are used to demonstrate the recombination dynamics in molecular beam epitaxy grown $\text{Al}_{0.85}\text{Ga}_{0.15}\text{As}_{0.56}\text{Sb}_{0.44}$ with temperature variation. Photoluminescence (PL) measurements at 8–50 K show that the bandgap varies from 1.547 to 1.527 eV. The radiative recombination processes in the alloy were found to be dictated by the complexities of antimony (Sb) incorporation during the growth. Time-resolved PL (TRPL) measurements show a change in initial carrier lifetimes of $\sim 3.5 \mu\text{s}$ at 8 K to $\sim 1 \mu\text{s}$ at 30 K. The knowledge of carrier dynamics from optical characterization methods such as PL and TRPL can be employed to contribute to shorter feedback loops for improvement of alloy fabrication in addition to enhancing growth processes.

© 2023 Author(s). All article content, except where otherwise noted, is licensed under a Creative Commons Attribution (CC BY) license (<http://creativecommons.org/licenses/by/4.0/>). <https://doi.org/10.1063/5.0145051>

Tremendous advances in semiconductor growth technology and III-Sb compound¹ physics in recent years have elicited the fabrication of excellent quality complex Sb alloys such as $\text{Al}_{1-x}\text{Ga}_x\text{As}_{1-y}\text{Sb}_y$. The simultaneous tailoring of all four components of the quaternary stoichiometry enables fine-tuning of the bandgap for near-infrared operations, while independent control of the lattice constant for lattice-matched growth is maintained (e.g., in GaSb and InP²). Molecular beam epitaxy (MBE) grown AlGaAsSb is extremely versatile, with applications ranging from barriers for mid-IR quantum well lasers³ and diode lasers,^{4,5} to distributed Bragg reflectors (DBRs) for vertical-cavity surface-emitting lasers (VCSELs)^{6,7} and avalanche photodiodes (APDs).^{8,9}

In $\text{Al}_{0.85}\text{Ga}_{0.15}\text{As}_{0.56}\text{Sb}_{0.44}$ APDs, desirable features such as high tolerance to temperature fluctuations,¹⁰ superior low noise characteristics,^{11–13} and large gain-bandwidth products of >400 GHz¹⁴ have been demonstrated. Recently, a thick $\text{AlAs}_{0.56}\text{Sb}_{0.44}$ avalanche region was also reported as having the lowest excess noise in the 1550 nm region.¹⁵ With 0.85 Al composition, the bandgap is predicted to be indirect and radiative recombination is expected to

occur from the X-valley¹⁶ (instead of Γ -valley in the direct bandgap semiconductors). Probing the lowest electron population level in the alloy with spectroscopy techniques, such as photoluminescence (PL) and time-resolved PL (TRPL), is essential to determine the optical properties significant for their application in devices.

Notwithstanding a limited susceptibility to the thermodynamics of surface atomic bonding in MBE-grown structures, the parameter growth window for III-AsSb systems remains inflexible due to the inherent complexities surrounding Sb incorporation.^{17–20} For instance, As-Sb exchange is highly temperature-dependent²¹ and has a non-unity sticking coefficient.²² As a result, the growth of III-AsSb entails careful maneuvering of various parameters.²³ Despite these efforts, the ideal stoichiometric ratio is inevitably affected in intricate quaternary composites, leading to the segregation of Sb. Here, PL characterization would enable the identification of spectral components, providing valuable information on the formation kinetics of the alloy.

In this work, low-temperature PL and time-resolved PL of the indirect bandgap E_g^X in $\text{Al}_{0.85}\text{Ga}_{0.15}\text{As}_{0.56}\text{Sb}_{0.44}$ are discussed.

The AlGaAsSb sample was grown using MBE at the University of Sheffield on a semi-insulating InP substrate. The wafer consisted of a 200 nm InGaAs buffer layer (lattice matched to AlGaAsSb), a 500 nm thick AlGaAsSb bulk layer, and finally a 20 nm thick InGaAs capping layer (to prevent oxidation of Al).

Figure 1(a) shows the intensity normalized temperature-dependent PL spectra of the AlGaAsSb bulk layer for temperatures from 8 to 50 K. The inset of integrated intensity at the same temperature range was obtained at 0.4 mW with a 650 nm PicoQuant laser diode coupled to an external frequency generator to enable a large range of pulse repetition rates. For PL, a high frequency of 80 MHz was used.

In Fig. 1(a), the spectral feature related to the AlGaAsSb alloy in the figure has two components labeled x_1 and x_2 . Here, the broader full width at half maximum (FWHM) and lower relative intensity of x_2 are attributed to the energy potential of the dissociated Sb during alloy growth. As a consequence of quaternary growth kinetics, x_2 is also expected to be rife with localized defect states.^{24,25} The feature at 1.33 eV (1.4 eV at 50 K) is PL emission from the InP substrate. From the inset, an abrupt drop in the intensity can be observed in the overall AlGaAsSb spectral intensity from 8 to 50 K.

In Fig. 1(b), the peak positions and FWHM from Fig. 1(a) are plotted. The two spectral components could not be separated or fitted reliably with Gaussian functions, suggesting that there is no distinct allocation of x_1 and x_2 states within the energy gap. Nevertheless, the average value of the two components shows a 20 meV temperature-induced bandgap reduction over 42 K (8–50 K). A 13 meV broadening of the FWHM additionally outlines the range of carrier redistribution energies in the indirect bandgap, with relatively low increments in temperature indicating shallow barriers between x_1 and x_2 .

From PL experiments, the indirect bandgap energy was detected at 1.547 eV. This value is close to values estimated from spectral response measurements, i.e., 1.56 eV for the indirect bandgap and 1.77 eV for the direct bandgap.¹⁶

The complete quenching of PL intensity at relatively low temperatures (Fig. 1) has been observed in indirect bandgap GaAsP²⁶ and SiGe^{27,28} alloys with disorder and is the result of fluctuations in the band edges that create traps for the recombining $e-h$ pairs. As the charge carriers here are subject to localization below a certain energetic “mobility edge,” annihilation of carriers occurs through

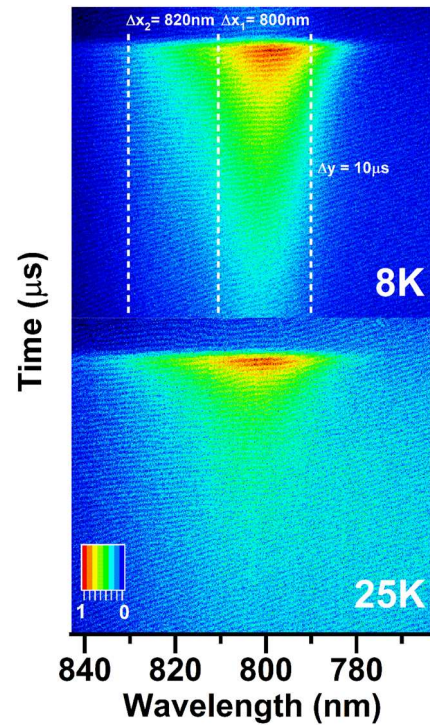


FIG. 2. Streak images of $\text{Al}_{0.85}\text{Ga}_{0.15}\text{As}_{0.56}\text{Sb}_{0.44}$ bulk at 8 and 25 K. The color legend indicates the relative intensity of the photons impinging the photocathode. Note that post-experimental image processing techniques were not applied to demonstrate the exact relative intensities between the two images; the wavelength scale is reversed in the x axis as higher energy photons are measured first in the streak camera.

non-radiative recombination even with the acquisition of low levels of thermal energy. Considering the complexities of AlGaAsSb growth and the separation of the spectral components, this is highly probable.

Time-resolved PL experiments were performed at 8–30 K by using the same 650 nm wavelength excitation source but

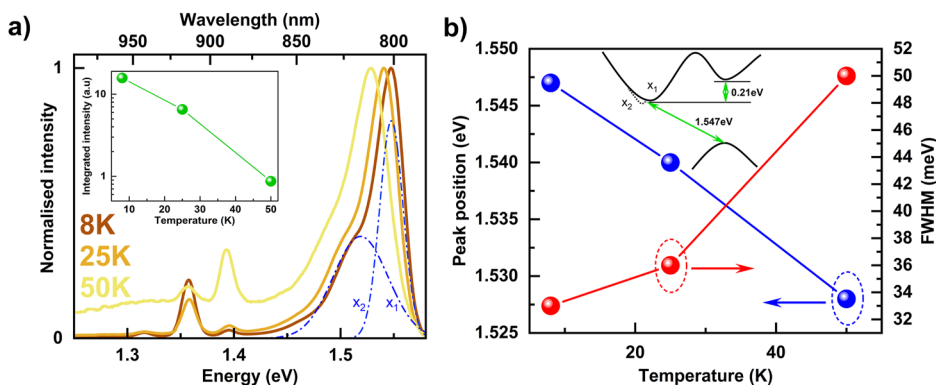


FIG. 1. (a) Temperature-dependent PL spectra of the $\text{Al}_{0.85}\text{Ga}_{0.15}\text{As}_{0.56}\text{Sb}_{0.44}$ alloy with inset of the integrated intensity of collective x_1 and x_2 peak. (b) The trend in peak positions and FWHM with temperature. The k -space depiction of the alloy band structure in its ground state is drawn in the inset with energy values obtained from PL and bandgap extrapolations.¹⁶

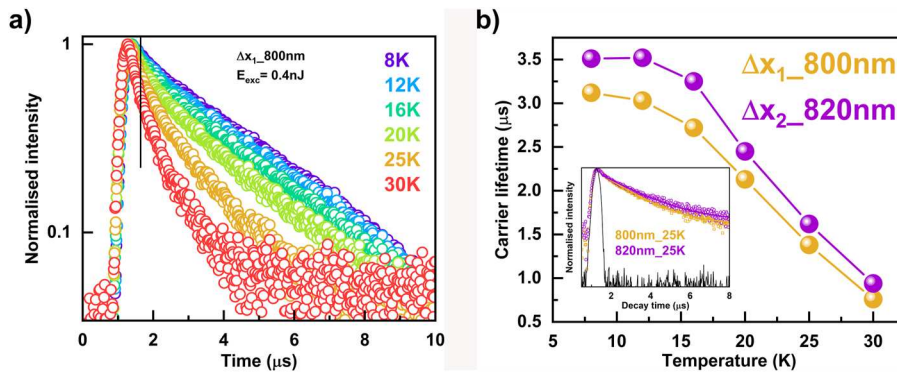


FIG. 3. (a) Monoexponential decay curves from 8 to 30 K measured for x_1 (black line indicates the contribution from laser pulse excluded from decay curve fits). (b) Plot of carrier lifetime of the two spectral components. The inset shows the decay curves of x_1 and x_2 at 25 K alongside the laser pulse decay measured in the same time window for comparison.

operated at low-frequency repetitions of 100 kHz (pulse energy of 0.4 nJ). Streak camera images evincing optical emission evolution times in the indirect AlGaAsSb bandgap at 8 and 25 K are shown in Fig. 2. The narrow streak camera capture window (765–845 nm) excluded any PL overlap from the InGaAs layers.

To improve the signal-to-noise ratio due to the rapid quenching of PL intensity, images were obtained using a photon counting method with long acquisition times. The 20 nm range used to extract decay times of the two spectral components x_1 (PL peak position at 800 nm) and x_2 (PL peak position at 820 nm) is indicated. In the top image for $T = 8$ K, the signal-to-noise ratio is excellent with long emission decays spanning the entire 10 μ s time range in the x axis. Upon increasing T to 25 K in the bottom image, the PL intensity diminishes considerably and the emission decay becomes much shorter. After 30 K, the decay curves could not be extracted anymore despite the long acquisition times used.

Microsecond-long decay times obtained with TRPL for the AlGaAsSb alloy are consistent with those observed for indirect bandgaps in other bulk semiconductor systems.^{29–31} The monoexponential decay traces for x_1 from 8 to 30 K in Fig. 3(a) exhibit a progressive truncation of the indirect radiative recombination channel with temperature. The single decay channel implies that radiative recombination occurs only from E_g^X without substantial carrier migration between the two spectral components at the measured temperature range (8–30 K). The decay times were extracted by fitting single exponential decay functions to the data for x_1 and x_2 in Fig. 3(a). These values are plotted in Fig. 3(b). Carrier lifetimes of ≤ 3.5 μ s at 8 K decrease significantly with temperature after 16 K to ~ 1 μ s at 30 K.

In conclusion, the optical properties of bulk Al_{0.85}Ga_{0.15}As_{0.56}Sb_{0.44} alloy have been evaluated at 8–50 K. By using low-temperature PL measurements, the two spectral components observed in the indirect bandgap were attributed to diversity in the quaternary alloy composition. The complete quenching of luminescence intensity at $T = 50$ K is related to a thermally induced carrier transfer to the nearby Γ -point valley. Monoexponential decay times of the order of microseconds signifying single radiative recombination channels from the E_g^X valley was also ascertained with temperature-dependent TRPL experi-

ments up to 30 K. The data presented here will be applied to further characterization and optimization of crystalline quality in AlGaAsSb alloys.

This work was supported by the European Union H2020 Marie Skłodowska-Curie Actions (Grant No. H2020-MSCA-ITN-2014-641899).

AUTHOR DECLARATIONS

Conflict of Interest

The authors have no conflicts to disclose.

Author Contributions

Shumithira Gandan: Data curation (lead); Writing – original draft (lead). **Lucas L. G. Pinel:** Resources (lead); Writing – review & editing (supporting). **Juan S. D. Morales:** Methodology (equal). **Jo Shien Ng:** Supervision (equal); Writing – review & editing (equal). **Chee Hing Tan:** Supervision (equal); Writing – review & editing (equal). **Tomasz J. Ochalski:** Supervision (equal); Writing – review & editing (equal).

DATA AVAILABILITY

The data that support the findings of this study are available from the corresponding author upon reasonable request.

REFERENCES

- H. Asahi, Y. Horikoshi, and E. Tournie, *Molecular Beam Epitaxy* (Wiley, 2019), p. 233.
- S. Adachi, *Springer Handbooks* (Springer, 2017), p. 1.
- W. Lei and C. Jagadish, *J. Appl. Phys.* **104**, 91101 (2008).
- L. Shterengas, G. Belenky, T. Hosoda, G. Kipshidze, and S. Suchalkin, *Appl. Phys. Lett.* **93**, 011103 (2008).
- S. D. Sifferman, H. P. Nair, R. Salas, N. T. Sheehan, S. J. Maddox, A. M. Crook, and S. R. Bank, *IEEE J. Sel. Top. Quantum Electron.* **21**, 1 (2015).
- D. Sanchez, L. Cerutti, and E. Tournié, *J. Phys. D: Appl. Phys.* **46**, 495101 (2013).

- ⁷C. Manz, Q. Yang, M. Rattunde, N. Schulz, B. Rösener, L. Kirste, J. Wagner, and K. Köhler, *J. Cryst. Growth* **311**, 1920 (2009).
- ⁸J. Li, A. Dehzangi, G. Brown, and M. Razeghi, *Sci. Rep.* **11**, 7104 (2021).
- ⁹S. Lee, B. Guo, S. H. Kodati, H. Jung, M. Schwartz, A. H. Jones, M. Winslow, C. H. Grein, T. J. Ronningen, J. C. Campbell, and S. Krishna, *Appl. Phys. Lett.* **120**, 71101 (2022).
- ¹⁰S. Abdullah, C. H. Tan, X. Zhou, S. Zhang, L. Pinel, and J. S. Ng, *Opt. Express* **25**, 33610 (2017).
- ¹¹J. Taylor-Mew, V. Shulyak, B. White, H. T. Chee, and J. S. Ng, *IEEE Photonics Technol. Lett.* **33**, 1155 (2021).
- ¹²L. L. G. Pinel, S. J. Dimler, X. Zhou, S. Abdullah, S. Zhang, C. H. Tan, and J. S. Ng, *Opt. Express* **26**, 3568 (2018).
- ¹³Y. Cao, T. Blain, J. D. Taylor-Mew, L. Li, J. S. Ng, and C. H. Tan, *Appl. Phys. Lett.* **122**, 051103 (2023).
- ¹⁴S. Xie, X. Zhou, S. Zhang, D. J. Thomson, X. Chen, G. T. Reed, J. S. Ng, and C. H. Tan, *Opt. Express* **24**, 24242 (2016).
- ¹⁵X. Yi, S. Xie, B. Liang, L. W. Lim, J. S. Cheong, M. C. Debnath, D. L. Huffaker, C. H. Tan, and J. P. R. David, *Nat. Photonics* **13**, 683 (2019).
- ¹⁶X. Zhou, S. Zhang, J. P. R. David, J. S. Ng, and C. H. Tan, *IEEE Photonics Technol. Lett.* **28**, 2495 (2016).
- ¹⁷A. N. Semenov, V. S. Sorokin, V. A. Solov'ev, B. Y. Mel'tser, and S. V. Ivanov, *Semiconductors* **38**, 266 (2004).
- ¹⁸A. Jasik, J. Kubacka-Traczyk, K. Regiski, I. Sankowska, R. Jakiea, A. Wawro, and J. Kaniewski, *J. Appl. Phys.* **110**, 073509 (2011).
- ¹⁹E. Selvig, B. O. Fimland, T. Skauli, and R. Haakenaasen, *J. Cryst. Growth* **227–228**, 562 (2001).
- ²⁰G. Almuneau, E. Hall, S. Mathis, and L. A. Coldren, *J. Cryst. Growth* **208**, 113 (2000).
- ²¹H.-R. Blank, S. Mathis, E. Hall, S. Bhargava, A. Behres, M. Heuken, H. Kroemer, and V. Narayanamurti, *J. Cryst. Growth* **187**, 18 (1998).
- ²²A. N. Semenov, V. A. Solov, B. Ya Mel, V. S. Sorokin, S. V. Ivanov, and P. S. Kop, in 9th International Symposium on Nanostructures: Physics and Technology, 2001.
- ²³T. Zederbauer, A. M. Andrews, D. MacFarland, H. Detz, W. Schrenk, and G. Strasser, *APL Mater.* **5** (2017).
- ²⁴M. Milanova, V. Donchev, K. L. Kostov, D. Alonso-Álvarez, E. Valcheva, K. Kirilov, I. Asenova, I. G. Ivanov, S. Georgiev, and N. Ekins-Daukes, *Semicond. Sci. Technol.* **32**, 085005 (2017).
- ²⁵O. Kwon, Y. Lin, J. Boeckl, and S. A. Ringel, *J. Electron. Mater.* **34**, 1301 (2005).
- ²⁶M. Oueslati, M. Zouaghi, M. E. Pistol, L. Samuelson, H. G. Grimmeiss, and M. Balkanski, "Photoluminescence study of localization effects induced by the fluctuating random alloy potential in indirect band-gap GaAs_{1-x}P_x," *Phys. Rev. B* **32**, 8220 (1985).
- ²⁷L. C. Lenchyshyn, M. L. W. Thewalt, J. C. Sturm, P. V. Schwartz, E. J. Prinz, N. L. Rowell, J. P. Noël, and D. C. Houghton, *Appl. Phys. Lett.* **60**, 3174 (1992).
- ²⁸U. Menczgar, G. Abstreiter, J. Olajos, H. Grimmeiss, H. Kibbel, H. Presting, and E. Kasper, *Phys. Rev. B* **47**, 4099 (1993).
- ²⁹R. N. Hall, *Phys. Rev.* **87**, 387 (1952).
- ³⁰R. Z. Bachrach and B. W. Hakki, *J. Appl. Phys.* **42**, 5102 (1971).
- ³¹Y. Li, R. Clady, A. F. Marshall, J. Park, S. V. Thombare, G. Chan, T. W. Schmidt, M. L. Brongersma, and P. C. McIntyre, *ACS Photonics* **2**, 1091 (2015).